Suppression of thermoacoustic instability by targeting the hubs of the turbulent networks in a bluff-body stabilized combustor (Supplementary Material)

Abin Krishnan†, R. I. Sujith, Norbert Marwan and Jürgen Kurths

1. Turbulent networks upstream of the bluff body during thermoacoustic instability

To focus on the formation of the large-scale vortical structure downstream of the dump plane better, we perform high-speed PIV just downstream of the dump plane. The region of interest is located just downstream of the dump plane, slightly above the bluff body shaft with a physical dimension of 50 mm $\times$ 36 mm. In this case, the number of nodes (N) is 2728 (refer the supplementary material of Krishnan *et al.* (2019) for further details). In figure 1, we examine the spatial distribution of the node strength (s) during one acoustic cycle during thermoacoustic instability. We note that the roll-up of the large-scale vortical structure is better captured here compared to the turbulent networks during thermoacoustic instability where the region of interest for the analysis of PIV is around the bluff body (refer figure 9) . The roll-up of the vortical structure immensely wrinkles the flame. Recently, Raghunathan *et al.* (2020), using multifractal analysis, showed that the roll-up of the flame by the large-scale vortical structure gives

† Email address for correspondence: abin.roja@gmail.com

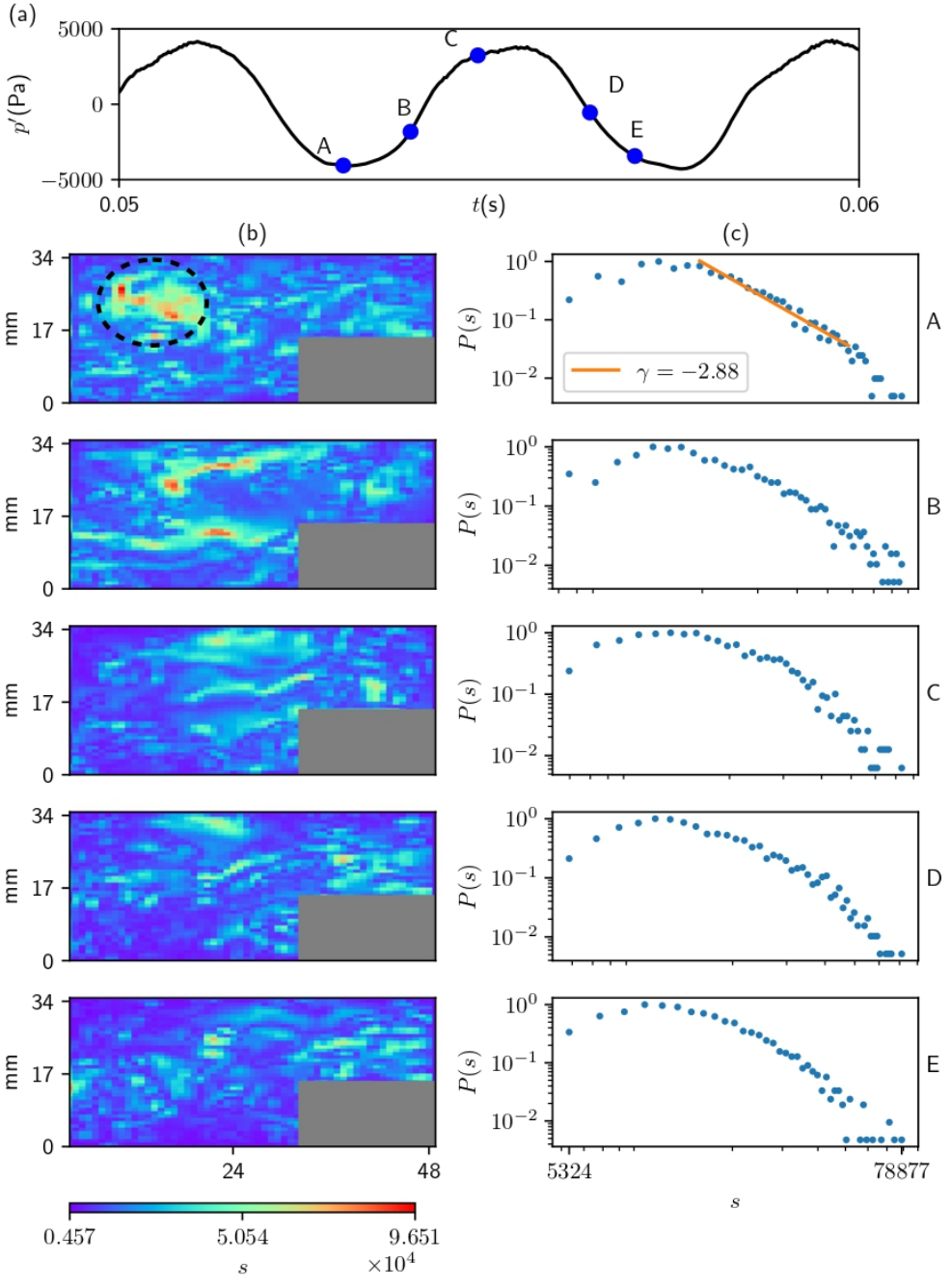

Figure 1: (b)The spatial distribution of the node strength, s, for the region just downstream of the dump plane during the time instants $A - E$ marked on (a) the time series of acoustic pressure during one acoustic cycle of thermoacoustic instability. (c) The power law exponent suggests that the large-scale vortical structure is the primary hub (encircled) of the weighted scale-free network.

the flame a space-filling nature. We observe that these large scale-vortical structures act as the hubs of the weighted scale-free networks (figure 1 (c), at time instant A).

Appendix A. Statistical analysis of the vorticity networks

To obtain a statistical significance of the vorticity network topologies, we analyzed 100 vorticity networks for each of the dynamical states of combustor operation, namely, combustion noise, intermittency (both aperiodic and periodic regimes), thermoacoustic instability and the state where thermoacoustic instability is suppressed with a steady air jet injection (written as suppressed state in coulmn 1 of table 1). During thermoacoustic instability, the 100 vorticity networks (obtained from 100 PIV images, respectively) correspond to around 14 acoustic cycles.

We analyzed the probability of the node strength distribution ($P(s)$ vs s) for all the 100 vorticity networks, one-by-one. Firstly, we examined whether we were able to successfully fit a line to the histogram plots of the node strength distribution. We note that the probability of the node strength distribution exhibited an inverse power law behaviour for around 85% for all cases except the suppressed state (column 2 of Table 1). The minimum, maximum, median, mean and standard deviation of the so obtained inverse-power law exponents are mentioned in columns 3-7, respectively. The median and mean values of the exponents are between 2 and 3 for all the cases. The standard deviation of the power-law exponents is low for combustion noise and the suppressed state as compared to intermittency (both aperiodic and periodic epochs) and thermoacoustic instability. In the final column, we examined the weighted scale-free nature of the vorticity network by calculating the number of vorticity networks with a power law exponent between 2 and 3. For example, during combustion noise, we could clearly observe an inverse power-law

Combustor states	**networks with a power law**	**Min**	**Max**	**Median**	**Mean**	**Std. devn.**	**scale free networks** (%)
Combustion noise	88	-3.27	-1.91	-2.25	-2.30	0.28	92.05
Intermittency (aperiodic)	85	-5.26	-1.40	-2.09	-2.30	0.76	61.18
Intermittency (periodic)	84	-4.32	-1.28	-2.37	-2.48	0.72	51.19
Thermoacoustic instability	85	-5.22	-1.62	-2.91	-2.94	0.70	54.12
Suppressed state	69	-2.95	-1.62	-2.00	-2.08	0.33	52.17

Table 1: The variation of the statistical properties of the power-law exponents of turbulent networks across the different states of combustor operation. We analysed 100 turbulent networks for each of the dynamical states of combustor operation.

distribution in 88 vorticity networks (column 1). Out of these 88 networks, we find that 81 networks are weighted scale-free (92.05%).

The intermittent appearance, disappearance and reappearance of weighted scale-free topology in turbulent networks, based on the Biot-Savart law, during the occurrence of thermoacoustic instability has been reported earlier in a swirl stabilized combustor (Murayama *et al.* 2018). In the current study, we find that the weighted scale-free network topology appears intermittently during all the states of combustor operation. Further, we also note that the weighted scale-free network topology is predominantly observed only during the state of combustion noise.

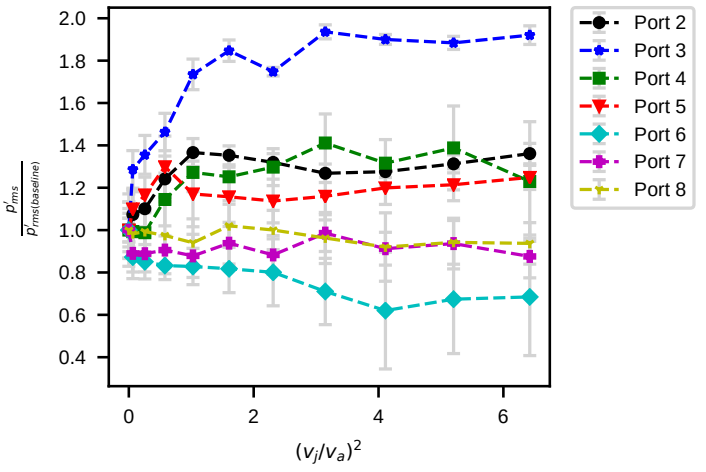

Figure 2: The variation of $p\prime_{rms}$ (normalized) of thermoacoustic oscillations due to a secondary air jet injection through single ports along the length of the combustor with respect to the total momentum flux ratio $(v_j/v_a)^2$. The vertical error bars represent the standard deviation.

Appendix B. Effect of steady air jet injection through single ports

Figure 2 summarises the effect of secondary steady air jet injection through each of the seven ports, numbered 2 to 8 (figure 10), at the top and bottom walls of the combustor. We find that thermoacoustic instability is not suppressed with a steady air jet injection through ports 2, 3, 4 and 5 even though we are able to successfully suppress thermoacoustic instability with combined injection through the above mentioned ports, namely, (a) ports 2 and 3 and (b) ports 4 and 5 (figure 11). Interestingly, the amplitude of the thermoacoustic oscillations increases with the injection of steady air jets through ports 2, 3, 4 and 5. At $(v_j/v_a)^2 = 6.42$, we observe an increase in $p\prime_{rms}$ with steady air jet injection through (a) port 2 ($\approx 36\%$ increase), (b) port 3 ($\approx 92\%$ increase), (c) port 4 ($\approx 24\%$ increase) and (d) port 5 ($\approx 25\%$ increase). The exact reason for this behaviour is unknown. One plausible reason could be that to successfully prevent the formation of the large-scale vortices downstream of the dump plane and at the tip of the bluff body, we may require to inject the jets through a pair of ports instead of a single port. We observe

a mild suppression of $p\prime_{rms}$ ($\approx 38\%$ decrease) with a steady air jet injection through port 6 (at $(v_j/v_a)^2 = 4.11$). There is not much effect with a steady air jet injection through ports 7 and 8; similar to the effect of the combined injection through ports 7 and 8 (figure 11).

REFERENCES

Krishnan, A., Manikandan, R., Midhun, P. R., Reeja, K. V., Unni, V. R., Sujith, R. I., Marwan, N. & Kurths, J. 2019 Mitigation of oscillatory instability in turbulent reactive flows: A novel approach using complex networks. *EPL (Europhysics Letters)* **128** (1), 14003.

Murayama, S., Kinugawa, H., Tokuda, I. T. & Gotoda, H. 2018 Characterization and detection of thermoacoustic combustion oscillations based on statistical complexity and complex-network theory. *Physical Review E* **97** (2), 022223.

Raghunathan, Manikandan, George, Nitin B, Unni, Vishnu R, Midhun, PR, Reeja, KV & Sujith, RI 2020 Multifractal analysis of flame dynamics during transition to thermoacoustic instability in a turbulent combustor. *Journal of Fluid Mechanics* **888**.